

Novel Features of Nuclear Chromodynamics

Stanley J. Brodsky¹

SLAC National Accelerator Laboratory
Stanford University, Stanford, CA, 94309

the date of receipt and acceptance should be inserted later

Abstract. I review a number of QCD topics where the nuclear environment provides new insights into fundamental aspects of the strong interactions. Quarks, gluons, and QCD in nuclear reactions

PACS. 2 4.85.+p

1 Introduction

One of the most challenging problems in QCD is to understand nuclei in terms of their fundamental quark and gluon degrees of freedom. Even the deuteron has exotic features such as its “hidden” color degrees of freedom. In this article I will review some new perspectives for nuclear physics, such as nuclear form factors and the nuclear force at short distances, which are consequences of fundamental features of QCD [1]. Conversely, the nuclear environment can bring new insights of hadron physics, such as “color transparency” The topics include novel effects such as flavor-dependent antishadowing and the breakdown of sum rules for nuclear structure functions.

2 Hadron and Nuclear Observables Light-Front QCD

Light-Front Quantization at fixed LF time $\tau = t+z/c$ (the “front form”) provides a rigorous formulation of hadron and nuclear physics, independent of the observer’s frame. A detailed review is given in ref. [2]. The spectroscopy of hadrons and nuclei can in principle be obtained as the bound state eigenvalues and eigensolutions of the QCD light-front Hamiltonian:

$$H_{LF}^{QCD} |\Psi_H\rangle = M_H^2 |\Psi_H\rangle .$$

Here $P^- = i \frac{d}{d\tau}$ is the light-front (LF) time $\tau = x^+ = t+z/c$ evolution operator, and the LF Hamiltonian $H_{LF} = P^+ P^- - P_{\perp}^2$ are derived directly from the QCD Lagrangian. The parameters $P^+ = P^0 + P^z$ and \mathbf{P}_{\perp} are kinematical and define the hadron’s four-momentum. The projection of the eigenstates on the free quark and gluon Fock basis $|n\rangle$ defines the light-front Fock state wavefunctions

$$\psi_n^H(x_i, \mathbf{k}_{\perp i}, \lambda_i)$$

where $\sum_i x_i = 1, \sum_i \mathbf{k}_{\perp i} = 0$. It is convenient to choose the “light-cone” gauge $A^+ = 0$ so that the gluons only have physical polarization $S^z = \pm 1$ and no ghosts appear. Remarkably, the $\psi_n^H(x_i, \mathbf{k}_{\perp i}, \lambda_i)$ LFWFs are independent of the hadron’s momentum P^+, \mathbf{P}_{\perp} . There is no Lorentz contraction of LFWFs [3,4]. The structure functions measured in deep inelastic scattering on a fixed target in the rest frame is the same structure function measured in an electron-ion collider. In fact, the LF formalism is Poincare’ invariant – all formulae are independent of the observer’s Lorentz frame.

The LF Heisenberg equation can be solved by matrix diagonalization for QCD(1+1). [5]. The LF vacuum is trivial for QCD – there are no vacuum condensates. In the case of the Standard Model, the usual Higgs VEV is replaced by a constant scalar field – a zero mode. [6]

Current matrix elements, such as electromagnetic, weak, and gravitational form factors of both hadrons and nuclei can be computed from the overlap of light-front wavefunctions [7,?,?] It is important to note that there is no formula analogous to the Drell-Yan-West LFWF overlap formula for current matrix elements using quantization in ordinary time t (the “instant form”) because of the necessity to include acausal, vacuum-induced currents.

The boost-invariant light-front wavefunctions (LFWFs) of the hadrons $\psi(x_i, \mathbf{k}_{\perp i}, \lambda_i)$, the eigensolutions of the QCD Light-Front Hamiltonian, are also the basis for computing the fundamental distributions E, H , etc., that underly Deeply Virtual Compton scattering [10]. The light-front formalism is also the basis for fundamental spin and other sum rules. The hadron and nuclear distribution amplitudes $\phi_H(x_i, Q)$ that appear in hard exclusive reactions are computed from the LFWFs integrated over the internal transverse momenta [11,12]; they obey DGLAP and ERBL evolution, respectively.

The hadronic and nuclear structure functions, transverse momentum distributions, etc., which are measured in deep inelastic lepton scattering (DIS) are based on the absolute squares of the LFWFs, modulo final-state

gluon exchange corrections which give the Bjorken-scaling leading-twist Sivvers pseudo-T-odd spin correlation [13] in deep inelastic lepton scattering as well as diffractive deep inelastic scattering (DDIS) [14] where the target remains intact. The Sivvers effect measures the pseudo T -odd correlation $i\mathbf{S} \cdot \mathbf{q} \times \mathbf{p}_Q$ of the target spin with the photon to quark jet production plane. The same interference of $L = 0$ and $L = 1$ amplitudes also enter the anomalous magnetic moment of the target. It would thus be particularly interesting to study the Sivvers effect of a polarized nuclear target.

3 Light-Front Holographic QCD

The spectroscopy of hadrons, together with their LFWFs, can be predicted using a novel nonperturbative approach to hadron physics – light-front (LF) holographic QCD [15–18]. AdS/QCD provides new analytical tools for hadron dynamics within a relativistic frame-independent color-confining first-approximation to the LF QCD Hamiltonian; the results follows from the mapping of the Hamiltonian equations in Anti-de Sitter (AdS) space to the relativistic semiclassical light-front bound-state equations in Minkowski space [16, 17], which is the boundary space of AdS₅. This connection gives an exact relation between the holographic variable z of AdS space and the invariant impact LF variable $\zeta = \sqrt{\frac{x}{1-x}}$ in physical space-time. This holographic connection also implies that the light-front effective potential $U \sim \kappa^2 \zeta^2$ in the LF Hamiltonian, corresponds to a modification of the infrared region of AdS space. The LFWFs of the hadrons can also be determined from AdS/QCD Light-Front Holography, as well as the meson and baryon spectroscopy and dynamics such as the meson and nucleon form factors.

The specific form of the LF potential $U \sim \kappa^2 \zeta^2$ in the LF Hamiltonian is determined by superconformal quantum mechanics [19–21, 18, 22, 23], which captures the relevant aspects of color confinement based on a universal emerging single mass scale $\kappa = \sqrt{\lambda}$ [24]. Only ratios are determined, such as $m_p/m_\rho = \sqrt{2}$ and $\Lambda_{\overline{MS}}/\kappa$ since QCD has no knowledge of MeV units. .

This novel nonperturbative approach to hadron physics predicts universal linear Regge trajectories and slopes in both orbital angular momentum and radial excitation quantum numbers. A massless pion appears in the limit of zero-mass quarks, and it gives remarkable connections between the light meson and nucleon spectra [23, 24]. The superconformal approach has thus the advantage that mesons and nucleons are treated on the same footing, and the confinement potential is uniquely determined by the formalism. Superconformal algebra leads to remarkable connections between the masses of mesons and baryons of the same parity supersymmetric relations between the bosonic and fermionic bound states of QCD [25]. Remarkably, AdS/QCD and Light-Front Holography, combined with superconformal algebra, predicts that the meson and Baryon Regge trajectories in n and L coincide if one shifts $L_M \rightarrow L_B + 1$. The baryons are bound states of a 3_C quark

and a $\bar{3}_C$ diquark cluster. One also predicts tetraquarks with the same masses as the baryons; they are identified as diquark antiquark bound states [25].

The analytic form of the QCD coupling $\alpha_s(Q^2) = \alpha_s(0) \exp(-Q^2/4\kappa^2)$ in the nonperturbative domain is also determined [26], consistent with effective charge phenomenology. One can also identify a transition scale Q_0 between perturbative and nonperturbative QCD.

4 The “Hidden Color” of Nuclear Wavefunctions

The deuteron is traditionally regarded in nuclear physics as a proton and neutron bound by a potential derived from pion and other meson exchange. However, from the standpoint of QCD, the deuteron is a composite of six 3_C color-triplet quarks [27]. One can in fact form five different color-singlet configurations from six color-triplet quarks, only one of which corresponds to the standard nuclear bound state two color-singlet nucleons; however, if the deuteron participates in a hard scattering reaction involving high transverse momentum such as elastic lepton-deuteron scattering or photodisintegration $\gamma d \rightarrow np$, all five color-singlet configurations will participate. In fact one can show that the five color-singlet configurations of the deuteron distribution amplitude $\phi_d(x, Q)$ evolve by ERBL evolution to equal weight at $Q^2 \rightarrow \infty$.

5 Cluster Decomposition of Nuclear Wavefunctions

The deuteron Light-Front wavefunction can be written as a convolution of the proton and neutron light-front wavefunction times a reduced two-body deuteron LFWF in the weak binding limit - a “cluster decomposition” valid for relativistic nuclear momenta [28, 29, 27] The deuteron form factors then have the factorization:

$$F_d(Q^2) = f_d^{\text{reduced}}(Q^2) \times F_p(Q^2/4) \times F_n(Q^2/4).$$

In effect, the dependence of the deuteron form factor reflecting nucleon compositeness is factorized out as an effective reduced form factor $f_d(Q^2)$. To first approximation, each nucleon scatters with momentum transfer $Q/2$.

6 The Asymptotic Behavior of the Form-Factors of Hadrons and Nuclei

The large- Q^2 behavior of the leading elastic form factors of a hadron or nucleus can be related by dimensional counting to the number n of its elementary constituents [30, 31]

$$F(Q^2) \propto \left(\frac{1}{Q^2}\right)^{n-1}.$$

In the case of the deuteron, the leading helicity-conserving form factors then falls as $A(Q^2) \sim \left(\frac{1}{Q^2}\right)^5$, and since $Q^4 F_N(Q^2) \sim$

const, the reduced form factor $f_d^{\text{reduced}}(Q^2)$ is thus predicted to fall as a monopole. This is verified experimentally [32]. The observed scaling of $Q^2 f_d^{\text{reduced}}(Q^2)$ implies that the nuclear potential (after removing the effects of nucleon structure) displays the scale-invariant behavior of a conformal theory. Its magnitude, much larger than expected from the small deuteron binding energy, indicating a sizeable contributions from hidden color degrees of freedom [27,33].

More generally, hard scattering cross sections in QCD obey the “dimensional counting rule”

$$\frac{d\sigma}{dt}(A + B \rightarrow C + D) = \frac{1}{s^{N-2}} \times F\left(\frac{p_T^2}{s}\right)$$

where $N = n_A + n_B + n_C + n_D = \sum_{i=1}^4 \tau_i$ is the total number of elementary fields which participate in the reaction. It is also the sum of the twist τ_i (dimension- spin) of the leading interpolating operators of each hadron or nucleus. This scaling is a fundamental property of hadron dynamics which follows nonperturbatively, from the light-front holographic principle of AdS/QCD [34,35], or from the near conformal properties of perturbative QCD; the asymptotic freedom behavior of quantum chromodynamics also leads to the counting rule behavior of hadronic and nuclear amplitudes at short distances.

7 The Nuclear Force at Short Distance

The angular dependence of hard scattering $pp \rightarrow pp$ cross section at high momentum transfer $p_T^2 = \frac{tu}{s}$ is consistent with the postulate that the dominant interaction at short distances occurs via the interchange of the common u and d quarks [36]. This is the analog of “spin exchange” (i.e., electron interchange) in atom-atom scattering. Quark interchange can be expressed as product of the LF wavefunctions of the incident and outgoing scattering hadrons and leads to an amplitude $T(pp \rightarrow pp) \propto \frac{\kappa^4}{u^2 t^2}$ and thus a cross section behaving at fixed center-of-mass angle θ_{CM} and fixed p_T^2/s which scales as $\frac{d\sigma}{dt} \propto \kappa^8/s^{10}$ [36] Here s , t , and u are the Mandelstam variables, and κ is the fundamental mass scale of QCD as derived from light-front holographic QCD. Thus quark interchange appears as the dominant QCD mechanism which underlies the nuclear force at short distances. It is analogous to the covalent bond underlying molecular binding in atomic physics.

8 Color Transparency

It is normally expected that a hadron scattering on the nucleons in a nucleus such as $pp \rightarrow pp$ elastic scattering can only occur on the $A^{1/3}$ peripheral nucleons since the incoming proton and outgoing nucleons will be suffer strong inelastic reactions or absorption. In fact, when the scattering reaction occurs at high momentum transfer, the reaction pp elastic scattering occurs undiminished on the Z protons of the nucleus: $d\sigma(pA \rightarrow pp(A-1)) = Zd\sigma(pp \rightarrow$

$pp)$. This phenomena, called “color transparency” occurs since the participating protons can only scatter and interact when their valence uud wavefunctions fluctuate to small color-octet configurations [37,38]. The small-size virtual configurations have negligible strong interactions are thus effectively transparent as they propagate through the nuclear domain. This remarkable phenomenon has also been observed and confirmed quantitatively in reactions such as diffractive dijet production $\pi A \rightarrow q\bar{q}X$ [39] and quasi-elastic electroproduction of vector mesons [40].

9 Anomalous Baryon to Meson Ratio in Heavy-Ion Collisions

Color transparency can explain the remarkable fact that the baryon production is observed to dominate meson production at high p_T in central heavy collisions $AA \rightarrow HX$ at RHIC [41]. For example a proton can be made directly, and efficiently, in a hard pQCD scattering subprocess such as $uu \rightarrow p\bar{d}$, rather than from the standard quark-quark hard-scattering reaction $qq \rightarrow qq$ and quark jet fragmentation process $q \rightarrow pq'$. In the case of fragmentation, there will be sizeable same-side energy requiring large values for the incident light-front momentum fractions x_1 and x_2 , where the structure function strengths are small. Thus direct production can dominate despite the higher power law suppression of the hard subprocess. In this case the produced proton is color transparent and suffers little final state absorption as it propagates out of the nuclear medium. The scaling behavior of the invariant production cross section at fixed $x_T = 2p_T/\sqrt{s}$ is also a powerful tool in order to probe the dynamics of particle production. A non-negligible contribution of higher-twist processes [42] in which the hadron is produced directly in the hard subprocess is needed to explain existing measurements.

10 Flavor-Dependent Nuclear Antishadowing

The shadowing and antishadowing of nuclear structure functions in the Gribov-Glauber picture is due respectively to the destructive and constructive interference of amplitudes arising from the multiple-scattering of quarks in the nucleus – two-step/one-step interference Glauber processes [43]. See fig. 1. The two-step reaction involves diffractive DIS on a front surface nucleon and then inelastic scattering on an interior nucleon. This two-step amplitude interferes destructively at small x with a usual one-step DIS amplitude for the DIS event on the second nucleon. The diffractive contributions to deep inelastic scattering includes Pomeron and Odderon contributions from multi-gluon exchange, as well as Reggeon quark-exchange contributions.

The coherence of multi-step nuclear processes leads to shadowing and antishadowing of the electromagnetic nuclear structure functions in agreement with measurements. Antishadowing arises from DDIS on the front nucleon of the two-step amplitude due to $I = 1$ Reggeon ex-

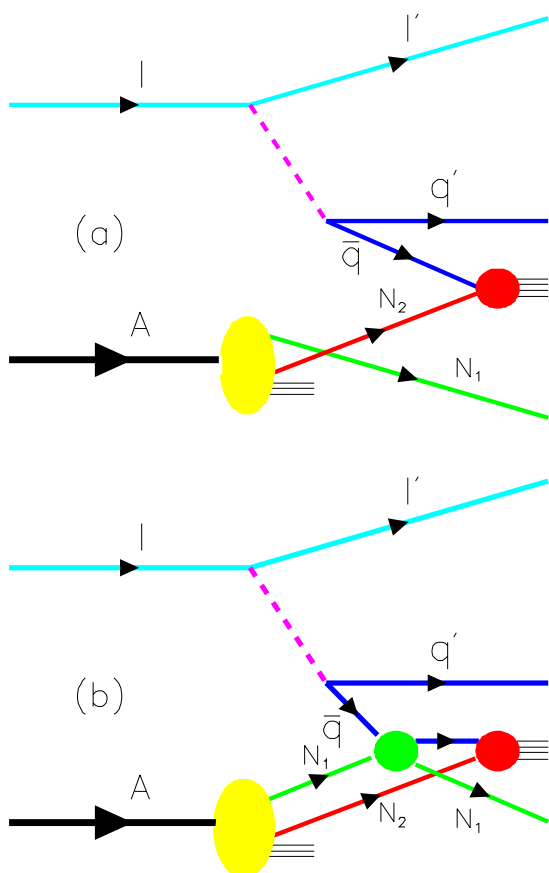


Fig. 1. Illustration of the interfering one-step and two-step processes that causes shadowing and antishadowing. In the case of Pomeron exchange, nucleon N_1 sees two beams with opposite phase, causing shadowing. In the case of Reggeon exchange, nucleon N_1 sees two beams with the same phase causing antishadowing.

change [44]. Each quark and antiquark flavor thus has different antishadowing[45]. See fig. 2. This picture thus leads to substantially different antishadowing for charged and neutral current reactions, thus affecting the extraction of the weak-mixing angle as well as explain why NuTeV does not see antishadowing in charged-current neutrino DIS on nuclei [46]. One also can have dependence of antishadowing on the polarization of the beam and target. It is thus important to check experimentally whether semi-inclusive deep inelastic scattering reactions on nuclei – where the struck quark flavor is tagged – have flavor-dependent antishadowing.

The fact that Reggeon couplings depend on the quantum numbers of the struck quark implies not only the non-universality of nuclear antishadowing for charged and neutral currents, but also a dependence of antishadowing on the polarization of the beam and target.

Shadowing and antishadowing are not properties of the nuclear LFWFs, but are a consequence of the lepton-nucleus reaction itself. The shadowed nucleons in the nuclear target are geometrically oriented transverse to the incident beam. In contrast, the nuclear LFWF, the eigen-solution of the QCD LF Hamiltonian, does not have knowledge of the orientation of the incident beam. Thus, the

physics of shadowing and antishadowing of nuclear structure functions is not contained in the LFWFs of nuclei. Furthermore, the two-step processes that causes shadowing and antishadowing involves propagation over a finite inter-nucleon separation – a spatial dependence which is contradiction to the usual assumption that the virtual photons in the forward virtual Compton amplitude $\gamma^* A \rightarrow \gamma^* A$ have vanishing separation $x^2 \rightarrow 0$ as $Q^2 \rightarrow \infty$. Clearly shadowing and antishadowing phenomena negate the usual assumptions required for the application of the Operator Product Expansion. If antishadowing is flavor dependent, it cannot compensate in sum rules with the deficits caused by flavor-independent shadowing. All of these considerations are incompatible with the derivation of momentum and charge sum rules for nuclear PDFs. There is thus no requirement that nuclear structure functions obey the usual momentum and charge sum rules.

11 Positronium-Nucleus Scattering

Doubly Virtual Compton scattering on a proton (or nucleus) can be measured for two *spacelike* photons $q_1^2, q_2^2 < 0$ with minimal, tunable, skewness ξ using positronium-proton scattering $[e^+e^-]p \rightarrow e^+e^-p'$. One can also mea-

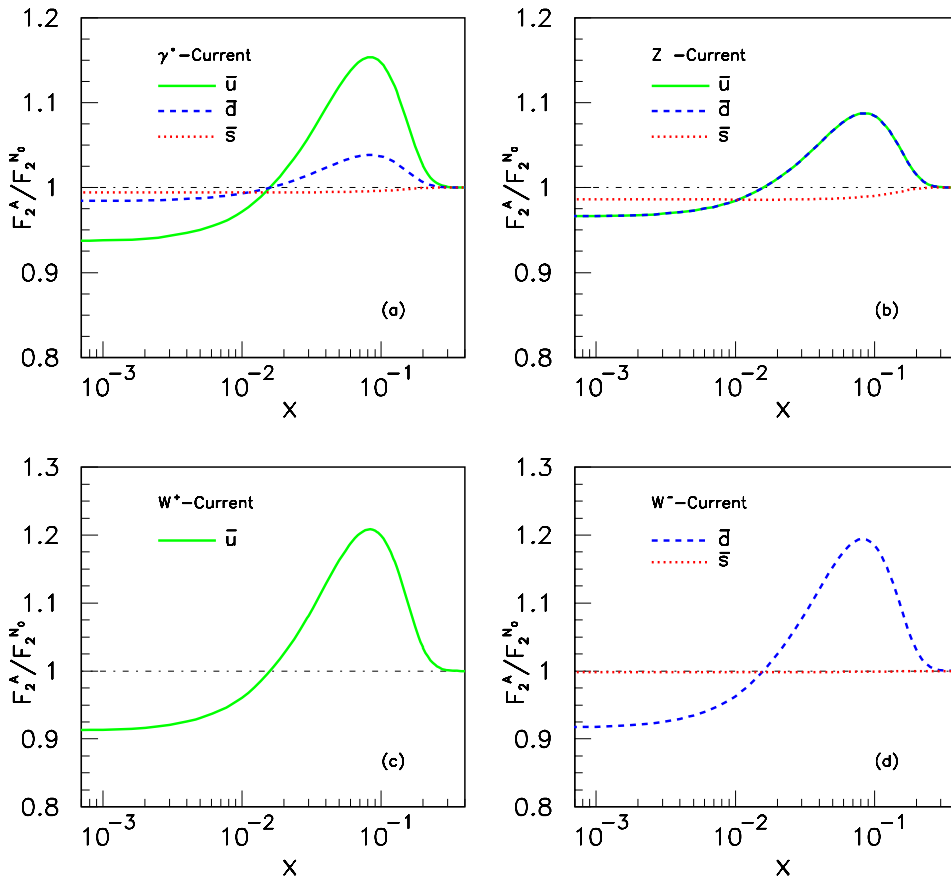


Fig. 2. Predictions for flavor-dependent antishadowing [45].

sure double deep-inelastic scattering and elastic positronium-dibaryon configurations allowed by QCD [49]. A dramatic proton scattering.

Relativistic positronium beams can be created using Bethe-Heitler e^+e^- pair production just below the e^+e^- continuum threshold. An analogous process will create the “true muonium” atom $[\mu^-\mu^-]$ [47,48].

Doubly Virtual Compton scattering on a proton (or nucleus) can be measured for two *spacelike* photons $q_a^2, q_b^2 < 0$ and with minimal, tunable skewness by using positronium-proton scattering $[e^+e^-]p \rightarrow e^+e^-p'$. This is illustrated in ?? The doubly virtual Compton amplitude on a nucleus

$$\gamma^*(q_a)A \rightarrow \gamma^*(q_b)A'$$

will also be affected by the same multiscattering processes that cause shadowing and antishadowing. See fig. 4. One can also measure double deep inelastic scattering reactions $[e^+e^-]p \rightarrow e^+e^-q'_a q_b X$, and coherent positronium-proton scattering $[e^+e^-]p \rightarrow [e^+e^-]p'$.

12 Novel Multiquark States: Hexaquarks and Octoquarks

The observation of a hadronic resonance d^* in the proton-neutron system with isospin $I = 0$ and spin-parity $J^P = 3^+$ raises the possibility of producing other novel six-quark

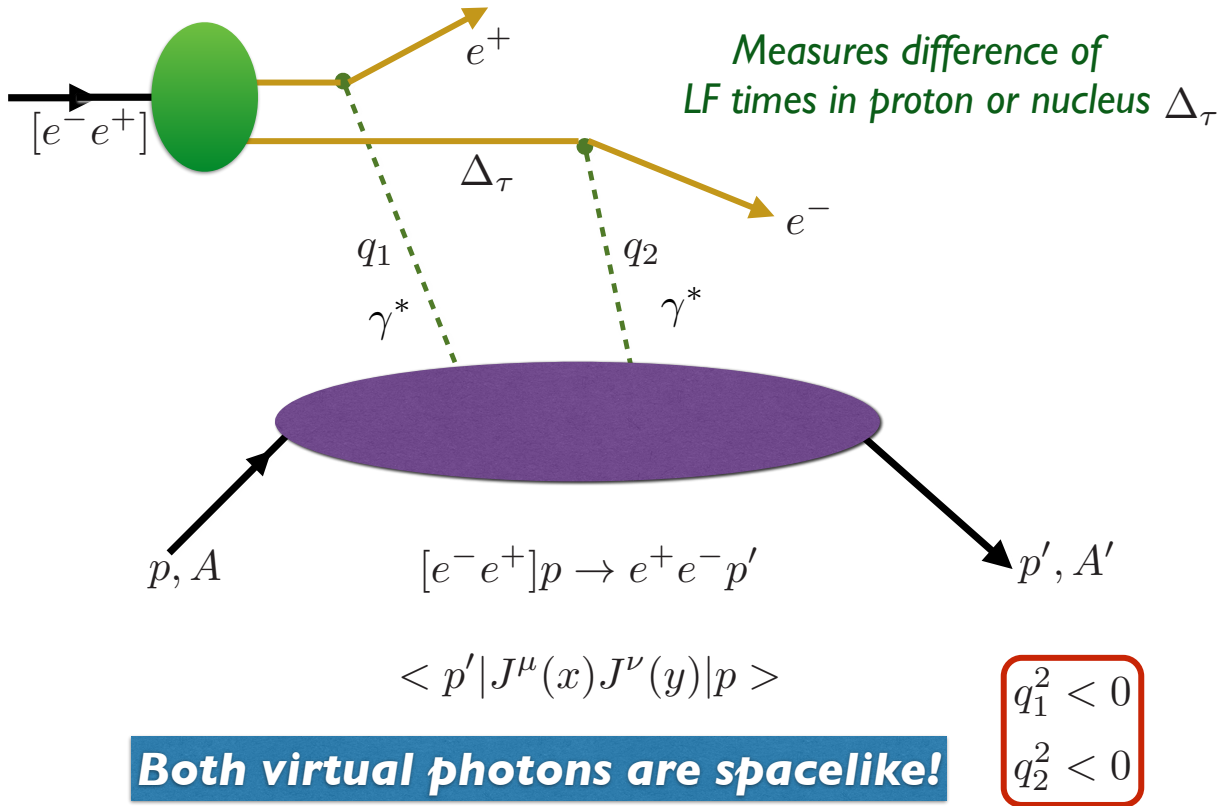
example of an exotic six-quark color-singlet system is the charge $Q = +4$, isospin $I = 3$, $I_z = +3$ $|uuuuuu\rangle$ state which couples strongly to $??^{++}??^{++}$. The width and decay properties of such hexaquark resonances could be regarded as manifestations of “hidden-color” six-quark configurations, a first-principle prediction of QCD – SU(3)-color gauge theory for the deuteron distribution amplitude.

The cross section for proton-proton elastic scattering at large momentum transfer $\frac{d\sigma}{dt}(pp \rightarrow pp)$ follows the pQCD prediction

$$s^{10} \frac{d\sigma}{dt}(pp \rightarrow pp) = F(\theta_{CM})$$

over the entire domain of hard scattering accessed by experiments. However, a measurement by Court et al. [50]s finds an unexpectedly large spin-spin correlation at $p_{lab} = 12.7$ GeV/c; i.e., $\sqrt{s} \simeq 5$ GeV, Remarkably, the cross section when both protons are polarized parallel and normal to the scattering plane rises rapidly to more than four times the cross section when the proton spins are antiparallel. This is the largest spin-spin correlation ever observed in hadron physics, strongly contradicting pQCD expectations [51] The color transparency of the $pp \rightarrow pp$ cross section disappears in the same kinematical region [52].

Measure Deeply Virtual Compton Scattering Using Positronium - Proton or Nucleus Scattering!



Both virtual photons are spacelike!

Fig. 3. Measurement of Doubly-Spacelike Virtual Compton Scattering using relativistic positronium beams. The two lepton-quark interactions occur at separate LF times. The imaginary part (unitary cut) of the $\gamma^* p \rightarrow \gamma^* p$ forward Compton amplitude gives the inelastic lepton proton cross section. The real part of the amplitude contains the $J = 0$ fixed pole from the LF instantaneous quark exchange interaction. The same double-spacelike amplitude contributes to the muonic hydrogen Lamb Shift. The inelastic positronium proton scattering amplitude $[e^+ e^-] p \rightarrow e^- e^+ X$ measures two-parton deep inelastic lepton-proton scattering.

Note that, $\sqrt{s} \simeq 5 \text{ GeV}$, is also the energy for producing hidden charm at threshold in the intermediate state—for example, the formation of a baryon number $B = 2$ octoquark, a hidden charm $|uuduudc\bar{c}\rangle$ resonance [53]. The natural quantum number in the pp amplitude for the lowest-mass resonance is $J = 1 = L = S$ with negative parity, given that the c and the \bar{c} have opposite parity. Remarkably, the protons can form this state only if the spins are parallel and transverse to the scattering plane. The interference of the resonance amplitude with the background quark-interchange amplitude provides a reasonable fit to the kinematic behavior of the $pp \rightarrow pp$ cross section at large angle.

The production cross section for charm at threshold in pp collisions is predicted to be $\sim 1\mu b$, which is compatible with unitarity and analyticity. It is clearly important to study its decay channels [54, 55]. A related $B = 2, Q = 1$ octoquark could appear in γd at $\sqrt{s} \simeq 5 \text{ GeV}$.

The original observation of the octoquark could be regarded as the first discovery of an exotic multiquark

state. Other octoquark states such as $|uuduuds\bar{s}\rangle$ and $|uuduudb\bar{b}\rangle$ should also exist.

13 Nuclear-Bound Quarkonium

QCD van der Waals interaction due to multiple gluon interactions are capable of binding heavy quarkonia to nuclei [56], such as the $J/\psi A$ bound states, composites of quarkonia and nuclei with no quarks in common. The octoquark $|uuduudQ\bar{Q}\rangle$ could be such a QCD bound state. The parameters of the potential can be estimated by identifying the multi-gluon exchange potential with the pomeron contributions to elastic meson-nucleon scattering. The gluonic potential can then be used to study the properties of nuclear-bound states. The probability of binding increases with nuclear number A since the non-relativistic kinetic energy carried by the nucleus decreases with increasing A .

8. G. B. West, Phys. Rept. **18**, 263 (1975). doi:10.1016/0370-1573(75)90035-6
9. S. J. Brodsky and S. D. Drell, Phys. Rev. D **22**, 2236 (1980). doi:10.1103/PhysRevD.22.2236
10. S. J. Brodsky, M. Diehl and D. S. Hwang, Nucl. Phys. B **596**, 99 (2001) doi:10.1016/S0550-3213(00)00695-7 [hep-ph/0009254].
11. G. P. Lepage and S. J. Brodsky, Phys. Rev. D **22**, 2157 (1980). doi:10.1103/PhysRevD.22.2157
12. V. L. Chernyak and A. R. Zhitnitsky, Phys. Rept. **112**, 173 (1984). doi:10.1016/0370-1573(84)90126-1
13. S. J. Brodsky, D. S. Hwang and I. Schmidt, Phys. Lett. B **530**, 99 (2002) doi:10.1016/S0370-2693(02)01320-5 [hep-ph/0201296].
14. S. J. Brodsky, P. Hoyer, N. Marchal, S. Peigne and F. Sannino, Phys. Rev. D **65**, 114025 (2002) doi:10.1103/PhysRevD.65.114025 [hep-ph/0104291].
15. S. J. Brodsky and G. F. de Teramond, Phys. Rev. Lett. **96**, 201601 (2006) doi:10.1103/PhysRevLett.96.201601 [hep-ph/0602252].
16. G. F. de Teramond and S. J. Brodsky, Phys. Rev. Lett. **102**, 081601 (2009) doi:10.1103/PhysRevLett.102.081601 [arXiv:0809.4899 [hep-ph]].
17. G. F. de Teramond, H. G. Dosch and S. J. Brodsky, Phys. Rev. D **87**, no. 7, 075005 (2013) doi:10.1103/PhysRevD.87.075005 [arXiv:1301.1651 [hep-ph]].
18. S. J. Brodsky, G. F. de Teramond, H. G. Dosch and J. Erlich, Phys. Rept. **584**, 1 (2015) doi:10.1016/j.physrep.2015.05.001 [arXiv:1407.8131 [hep-ph]].
19. V. de Alfaro, S. Fubini and G. Furlan, Nuovo Cim. A **34**, 569 (1976).
20. S. Fubini and E. Rabinovici, Nucl. Phys. B **245**, 17 (1984). doi:10.1016/0550-3213(84)90422-X
21. S. J. Brodsky, G. F. De Tramond and H. G. Dosch, Phys. Lett. B **729**, 3 (2014) doi:10.1016/j.physletb.2013.12.044 [arXiv:1302.4105 [hep-th]].
22. G. F. de Teramond, H. G. Dosch and S. J. Brodsky, Phys. Rev. D **91**, no. 4, 045040 (2015) doi:10.1103/PhysRevD.91.045040 [arXiv:1411.5243 [hep-ph]].
23. H. G. Dosch, G. F. de Teramond and S. J. Brodsky, Phys. Rev. D **91**, no. 8, 085016 (2015) doi:10.1103/PhysRevD.91.085016 [arXiv:1501.00959 [hep-th]].
24. S. J. Brodsky, G. F. de Tramond, H. G. Dosch and C. Lorc, Phys. Lett. B **759**, 171 (2016) doi:10.1016/j.physletb.2016.05.068 [arXiv:1604.06746 [hep-ph]].
25. S. J. Brodsky, G. F. de Tramond, H. G. Dosch and C. Lorc, Int. J. Mod. Phys. A **31**, no. 19, 1630029 (2016) doi:10.1142/S0217751X16300295 [arXiv:1606.04638 [hep-ph]].
26. S. J. Brodsky, G. F. de Tramond, A. Deur and H. G. Dosch, Few Body Syst. **56**, no. 6-9, 621 (2015) doi:10.1007/s00601-015-0964-1 [arXiv:1410.0425 [hep-ph]].
27. S. J. Brodsky, C. R. Ji and G. P. Lepage, Phys. Rev. Lett. **51**, 83 (1983). doi:10.1103/PhysRevLett.51.83
28. S. J. Brodsky and B. T. Chertok, Phys. Rev. Lett. **37**, 269 (1976). doi:10.1103/PhysRevLett.37.269
29. S. J. Brodsky and B. T. Chertok, Phys. Rev. D **14**, 3003 (1976). doi:10.1103/PhysRevD.14.3003
30. S. J. Brodsky and G. R. Farrar, Phys. Rev. D **11**, 1309 (1975). doi:10.1103/PhysRevD.11.1309
31. V. A. Matveev, R. M. Muradian and A. N. Tavkhelidze, Lett. Nuovo Cim. **7**, 719 (1973). doi:10.1007/BF02728133
32. S. Rock *et al.*, Phys. Rev. D **46**, 24 (1992). doi:10.1103/PhysRevD.46.24
33. S. J. Brodsky and G. F. de Teramond, Acta Phys. Polon. B **41**, 2605 (2010) [arXiv:1009.4232 [hep-ph]].
34. J. Polchinski and M. J. Strassler, Phys. Rev. Lett. **88**, 031601 (2002) doi:10.1103/PhysRevLett.88.031601 [hep-th/0109174].
35. S. J. Brodsky and G. F. de Tramond, Phys. Lett. B **582**, 211 (2004) doi:10.1016/j.physletb.2003.12.050 [hep-th/0310227].
36. J. F. Gunion, S. J. Brodsky and R. Blankenbecler, Phys. Rev. D **8**, 287 (1973). doi:10.1103/PhysRevD.8.287
37. S. J. Brodsky and A. H. Mueller, Phys. Lett. B **206**, 685 (1988). doi:10.1016/0370-2693(88)90719-8
38. L. Frankfurt, M. Strikman, M. Zhalov and B. Kopeliovich, Nucl. Phys. A **527**, 585C (1991). doi:10.1016/0375-9474(91)90161-X
39. E. M. Aitala *et al.* [E791 Collaboration], Phys. Rev. Lett. **86**, 4773 (2001) doi:10.1103/PhysRevLett.86.4773 [hep-ex/0010044].
40. D. Dutta, K. Hafidi and M. Strikman, Prog. Part. Nucl. Phys. **69**, 1 (2013) doi:10.1016/j.pnpnp.2012.11.001 [arXiv:1211.2826 [nucl-th]].
41. F. Arleo, S. J. Brodsky, D. S. Hwang and A. M. Sickles, Phys. Rev. Lett. **105**, 062002 (2010) doi:10.1103/PhysRevLett.105.062002 [arXiv:0911.4604 [hep-ph]].
42. F. Arleo, S. J. Brodsky, D. S. Hwang and A. M. Sickles, Nucl. Phys. Proc. Suppl. **207-208**, 81 (2010). doi:10.1016/j.nuclphysbps.2010.10.021
43. L. Stodolsky, Phys. Lett. B **325**, 505 (1994). doi:10.1016/0370-2693(94)90047-7
44. S. J. Brodsky and H. J. Lu, Phys. Rev. Lett. **64**, 1342 (1990). doi:10.1103/PhysRevLett.64.1342
45. S. J. Brodsky, I. Schmidt and J. J. Yang, Phys. Rev. D **70**, 116003 (2004) doi:10.1103/PhysRevD.70.116003 [hep-ph/0409279].
46. I. Schienbein, J. Y. Yu, K. Kovarik, C. Keppel, J. G. Morfin, F. Olness and J. F. Owens, Phys. Rev. D **80**, 094004 (2009) doi:10.1103/PhysRevD.80.094004 [arXiv:0907.2357 [hep-ph]].
47. S. J. Brodsky and R. F. Lebed, Phys. Rev. Lett. **102**, 213401 (2009) doi:10.1103/PhysRevLett.102.213401 [arXiv:0904.2225 [hep-ph]].
48. A. Banburski and P. Schuster, Phys. Rev. D **86**, 093007 (2012) doi:10.1103/PhysRevD.86.093007 [arXiv:1206.3961 [hep-ph]].
49. M. Bashkanov, S. J. Brodsky and H. Clement, Phys. Lett. B **727**, 438 (2013) doi:10.1016/j.physletb.2013.10.059 [arXiv:1308.6404 [hep-ph]].
50. G. R. Court *et al.*, Phys. Rev. Lett. **57**, 507 (1986). doi:10.1103/PhysRevLett.57.507
51. S. Brodsky, G. de Teramond and M. Karliner, Ann. Rev. Nucl. Part. Sci. **62**, 1 (2012) [Ann. Rev. Nucl. Part. Sci. **62**, 2082 (2011)] doi:10.1146/annurev-nucl-102711-094949 [arXiv:1302.5684 [hep-ph]].
52. J. Aclander *et al.*, Phys. Rev. C **70**, 015208 (2004) doi:10.1103/PhysRevC.70.015208 [nucl-ex/0405025].

53. S. J. Brodsky and G. F. de Teramond, Phys. Rev. Lett. **60**, 1924 (1988). doi:10.1103/PhysRevLett.60.1924
54. S. J. Brodsky, Eur. Phys. J. A **52**, no. 8, 220 (2016). doi:10.1140/epja/i2016-16220-1
55. S. J. Brodsky, SLAC-PUB-14985.
56. S. J. Brodsky, I. A. Schmidt and G. F. de Teramond, Phys. Rev. Lett. **64**, 1011 (1990). doi:10.1103/PhysRevLett.64.1011
57. S. J. Brodsky and R. F. Lebed, Phys. Rev. D **91**, 114025 (2015) doi:10.1103/PhysRevD.91.114025 [arXiv:1505.00803 [hep-ph]].